

SIMPLIFIED PREDICTION OF SOUND RADIATION DUE TO BENDING MODE RESONANCES OF SUBMERGED CYLINDERS

Roger Kinns^{1,2}, Hongjian Wu², Herwig Peters² and Nicole Kessissoglou²

¹RKAcoustics, Clynder, Helensburgh G84 0QQ, UK
Email: rogerkinns17@gmail.com

²School of Mechanical and Manufacturing Engineering
UNSW Australia, Sydney NSW 2052, Australia
Email: n.kessissoglou@unsw.edu.au

Abstract

The aim of this work is to explore the nature of radiation from bending modes of a submerged tube with variation in mass distribution along the length of the tube. The bending modes of a fluid-loaded tube are initially predicted using a simple finite element shell model, where the effects of water loading are modelled by adding mass to that of the tube itself. The sound radiation is then predicted using an array of transverse dipoles whose strengths are proportional to the local cross-sectional area and vibration amplitude. The effects of retarded time are taken into account for directions that are not normal to the tube. For comparison with the semi-analytical approach, a fully coupled finite element/boundary element model of the fluid-loaded tube was also developed. Results from both techniques show that variation of the mass distribution of the fluid-loaded tube has a large impact on the radiated sound power and directivity of the radiated sound pressure due to low order bending modes.

1. Introduction

Radiation from submerged shells has been described in general papers and textbooks that form a strong foundation for subsequent work [1,2]. The specific case of radiation from bending modes of a free-free beam was considered by Junger [3]. Recent work by the authors examined the effects of changing the buoyancy and aspect ratio of a rigid fluid-loaded shell on sound radiation [4]. Global modes and radiation characteristics of a submerged shell are altered by isolation of internal masses [5]. It was shown by Hartnell-Beavis and Swinbanks [6] that an array of soft mounts for a flexible machinery raft should be distributed to match the mass distribution of the mounted structure, in order to achieve minimum vertical hull excitation. The total mount force in the vertical direction due to a vertical force applied to the raft is then the same as for a rigid structure with identical total mass and mounting stiffness. There is a direct analogy with radiation from submerged, flexible shells due to a given applied force. Sound radiation from successive bending modes of a submerged shell might be minimised by matching the sectional buoyancy distribution to the longitudinal mass distribution. This is analogous to the static design of a ship or submarine for minimum vertical shear forces across longitudinal sections.

In this work, a simple fluid-loaded tube with variation in longitudinal mass distribution is used to explore the radiated sound due to low order bending resonances. The mechanical input power, and the radiated sound power and directivity of the far-field sound pressure, are predicted using both a semi-analytical approach and a numerical approach. The input power is determined from the product of the *rms* sinusoidal applied force and the *rms* component of velocity that is in-phase with that force.

Resonance of a particular mode is taken to correspond to a local input power maximum. The maxima are determined accurately using high resolution frequency analysis.

In the semi-analytical approach, the tube vibration is determined by assuming that the effective mass of each section of the tube is that of the tube itself plus an added mass of water. The radiated power is assumed to be much less than the mechanical input power, so that vibration is controlled by structural, not radiation, damping. The radiation is computed using a linear array of dipoles, where the source strength and phase of each dipole are derived from the operational deflection shape (ODS) of the tube and its local cross section. The ODS is computed using a simple finite element model of the tube transverse point force excitation applied at one end, where the tube mass is increased by the added mass of water. In the numerical approach, a fully coupled finite element/boundary element model of the fluid loaded tube was developed. In each model, variation in mass distribution along the length of the tube was considered. Predictions of the radiated sound power and directivity of the far-field sound pressure due to the first three successive bending mode resonances from the two approaches are compared.

2. Model Description and Choice of Parameters

Figure 1 shows a schematic diagram of a horizontal free-free tube with a force applied at one end in the vertical plane. This simulates the effect of a transverse hull force due to a propeller, transmitted via the propeller shaft and the pressure field in the fluid [7]. The applied end force is sinusoidal and has an amplitude of 1 N at radian frequency ω . The tube is modelled using shell elements.

The wavelength of underwater sound at the first bending mode of a floating or submerged hull is typically six times the hull length. For example, a 250m long cruise ship will have a first bending mode resonant frequency of about 1 Hz (1500m sound wavelength), while a submerged hull with 50m length may have a first bending mode frequency of about 5 Hz (300m wavelength). Submerged hulls tend to be stiffer in order to withstand water pressure, but also have heavier water loading. In the following analysis for a 45m long tube with a diameter of 1m, the material and geometric parameters for the cylinder have been chosen to give a first bending resonance at about 6 Hz, and are listed in Table 1. The density ρ_f and speed of sound in water c_f are 1000 kg/m^3 and 1500 m/s , respectively. The density and Young's modulus are chosen to ensure that the sound wavelength relative to the tube length at bending resonances is representative of full scale. The effects of retarded time in directions other than normal to the tube are then realistic. The loss factor η associated with structural damping is assumed to be 0.02 and is constant for the low frequency range considered here. Practical loss factors are usually higher and also tend to increase with frequency.

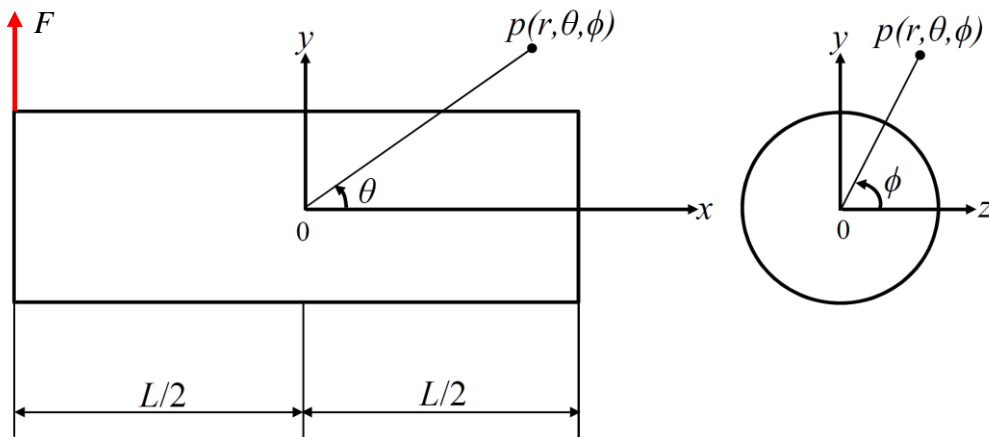


Figure 1. Schematic diagram of a horizontal tube with an applied end force in the vertical plane, showing the chosen spherical co-ordinate system with polar angle θ and azimuth angle ϕ

The mass distribution along the tube is varied using the parameter α , where the tube is divided into three sections: $L/4$, $L/2$ and $L/4$ long. The outer sections have mass per unit length $m_{c1} = m_{c3} = m_b(1 + \alpha)$, while in the centre section, $m_{c2} = m_b(1 - \alpha)$, where m_b is the average mass per unit length that corresponds to neutral buoyancy. If $\alpha = 0$, the mass per unit length is the same in each section. If $\alpha < 0$, the tube ends are relatively light. If $\alpha > 0$, the tube ends are relatively heavy. The distributions of mass are shown in Table 2 for the principal values of α .

Table 1. Geometric and material parameters for the tube

Parameter	Value	Unit
Length	45	m
Length of central section	22.5	m
Length of end section	11.25	m
Radius	0.5	m
Thickness	0.025	m
Young's modulus	2.1e12	Pa
Poisson's ratio	0.3	
Damping loss factor	0.02	
Density for neutral buoyancy	10,111.2	kg/m ³

Table 2. Variation in mass distribution

Central mass variation α	Density (kg/m ³)		
	Left	Central	Right
$\alpha = +0.4$	14000	6000	14000
$\alpha = 0$	10000	10000	10000
$\alpha = -0.4$	6000	14000	6000

3. Results for a Thin, Fluid-Loaded Tube

A segment of a thin, flexible tube has an acoustic reactance corresponding to an added mass of water, while its acoustic resistance is that of a rigid cylinder segment having the same vibration amplitude. This amplitude varies along the length of the cylinder. A bending mode of a water-loaded tube has shape $w(x)$ such that

$$\int_L m_e(x)w(x)dx = 0 \quad (1)$$

$m_e(x)$ is the effective mass per unit length of the fluid-loaded tube and is the summation of the actual mass per unit length of the tube, $m_c(x)$, and the added mass per unit length due to the surrounding fluid, $m_f(x)$

$$m_e(x) = m_c(x) + m_f(x) \quad (2)$$

The added mass due to the fluid loading is given by [8]

$$m_f(x) = \pi\rho_f a^2(x) \quad (3)$$

where $a(x)$ is the radius of the tube at location x along the tube. For simplicity, in this work, the radius of the tube is invariant along its length.

The radiation due to a vibrating tube segment with a rigid cross-section and unit length is that due to a dipole having the same volume, provided that the dimensions of the segment are small relative to the wavelength of underwater sound. Then, the sound pressure at large distance r and direction θ, ϕ in Fig. 1 due to a segment vibrating with amplitude $w(x)$ is [3]

$$p(r, \theta, \phi) = \frac{j\omega^3 \rho_f a^2(x) w(x) \sin \theta \sin \phi e^{-j\omega r \cos \theta / c_f}}{2c_f r} \quad (4)$$

If $\theta = 90^\circ$, the total pressure, obtained by integration along the length of the tube, is proportional to

$$\int_L a^2(x) w(x) dx = 0 \quad (5)$$

From Eq. (3), the added mass due to fluid loading is directly proportional to the cross-sectional area of the tube at each point along the tube axis. Thus, the total radiation normal to the tube ($\theta = 90^\circ$) for a pure bending mode is zero, if m_e / m_f is independent of location x along the tube. This is equivalent to a statement that the axial distribution of buoyancy should match the axial distribution of mass for minimum sound radiation due to bending modes in the direction normal to the tube.

4. Semi-Analytical Approach

The sound radiation due to bending vibration of a thin tube is approximated by a linear array of transverse dipoles, where the dipole strength is proportional to the vibration amplitude and the cross-sectional area of the tube at each location and frequency [3]. If end effects are ignored, the added mass of water is directly proportional to the cross-sectional area of the tube at each point along it. The far-field radiation in any direction can be computed by taking account of retarded time. The pressure field due to each dipole varies as $\sin \phi$ where ϕ is the angle of rotation about the longitudinal axis of the tube from the horizontal plane, as shown in Fig 1. The calculation of radiated sound power is then straightforward and results can be calculated very quickly.

The thin tube in water is modelled as a dry tube with added mass corresponding to the mass of displaced water at each section. It is anticipated that the radiated sound power at bending resonances is at least two orders of magnitude smaller than the input power. Then, the operational deflection shape (ODS) of the tube at resonance is hardly affected by sound radiation. This allows the tube to be modelled using a simple finite element (FE) analysis. The Patran/Nastran FE model of the thin tube has 240 longitudinal elements and 24 circumferential shell elements. The dipole strength is determined from the displacement of the tube axis. The ODS at each the first three bending resonances is a sequence of complex numbers, corresponding to displacement components that are in-phase and out-of-phase with the applied force.

The complex displacement of the m^{th} element in a linear array of N elements, where each element has length d and radius a_m , is w_m . The phase difference between the contributions from adjacent dipole sources is $k_f d \cos \theta$, corresponding to a time delay between the radiated sound signals from individual dipole sources if $\theta \neq 90^\circ$. The radiated far-field pressure at distance r from the array ($r \gg L$) is then

$$p_{\text{real}}(r, \theta, \phi) = \frac{j\omega^3 \rho_f d \sin \theta \sin \phi}{2c_f r} \sum_{m=0}^{N-1} a_m^2 w_m e^{-jmk_f d \cos \theta} \quad (6)$$

where $k_f = \omega / c_f$. The total radiated sound power from a linear array of dipole sources with varying amplitude can be computed semi-analytically by substituting equation (9) into the following equation [2,9]

$$\Pi = \int_0^{2\pi} \int_0^\pi \frac{|p(r, \theta, \phi)|^2}{2\rho_f c_f} r^2 \sin \theta d\theta d\phi \quad (7)$$

5. Numerical Approach

The FE mesh in the semi-analytical model was also used to represent the tube in the fully coupled finite element/boundary element (FE/BE) model. The surrounding fluid was now represented by the BE model. The FE model was created in MSC Patran/Nastran and the BE model was created in Sysnoise. The coupled FE/BE model was solved in Sysnoise. A total of 3276 quadrilateral shell elements were used at the interface between the tube and surrounding fluid, while retaining 5760 elements in the FE model. The same excitation force was applied at one end as in the semi-analytical model. Without explicit assumptions concerning dipole radiation and field characteristics, using the numerical approach, run times are much longer and it is more difficult to achieve convergence.

6. Results and Discussion

6.1 Peak input power frequencies

Results between the two approaches are compared in what follows in terms of resonant frequencies, ODSs, pressure fields in the plane of the cylinder and applied force, and the total radiated sound power. The resonant frequencies derived from the FE model are up to 3% lower than those computed from the FE/BE model, suggesting that the added mass of water is reduced in the FE/BE model by end effects. There is a weak variation in resonant frequencies with α . The peak frequencies at the first bending mode are respectively 3% higher for $\alpha = -0.4$ and 0.15% lower for $\alpha = +0.4$ than for $\alpha = 0$. The variations at the second bending mode are smaller than 1% for the range $-0.4 \leq \alpha \leq +0.4$. The variations at the third bending resonance are respectively 1.5% higher for $\alpha = -0.4$ and 0.5% lower for $\alpha = +0.4$ than for $\alpha = 0$.

6.2 Operational deflected shapes at peak input power

Figures 2 and 3 show the ODSs determined at the frequencies of peak input power for the first and third bending modes. The second bending mode is anti-symmetric. These results are derived from the 24×240 FE model of the tube using Patran/Nastran. They are almost identical to those derived from the FE/BE model. The amplitudes have been normalised to unity at the driven end for the displacement component that is out-of-phase with the applied force. Only the out-of-phase components are shown. The in-phase components are relatively small, but they lead to asymmetry of directivity patterns about $\theta = 90^\circ$.

6.3 Input power and radiated power

The variations of input power and radiated sound power with frequency are shown in Fig. 4 for $\alpha = -0.4, 0$ and $+0.4$. These results are derived from the fully coupled FE/BE model using Patran/Nastran and Sysnoise. The radiated sound power is at least 28 dB below the input power at the three resonant peaks, confirming that the radiated sound has negligible effect on the vibration amplitude at resonance. Almost all the input mechanical power is dissipated as heat, despite the low damping; the input power and radiated sound power are only equal when there is zero structural damping. The radiated sound power corresponds to that due to a dipole at low frequencies. The input power at resonance hardly changes with α , but the value of α has a large effect on the radiated sound. When $\alpha = 0$, all three fully-resolved peaks in radiated sound power are only about 10 dB above the power radiated by the dipole, due to the self-cancelling effects of the uniform tube.

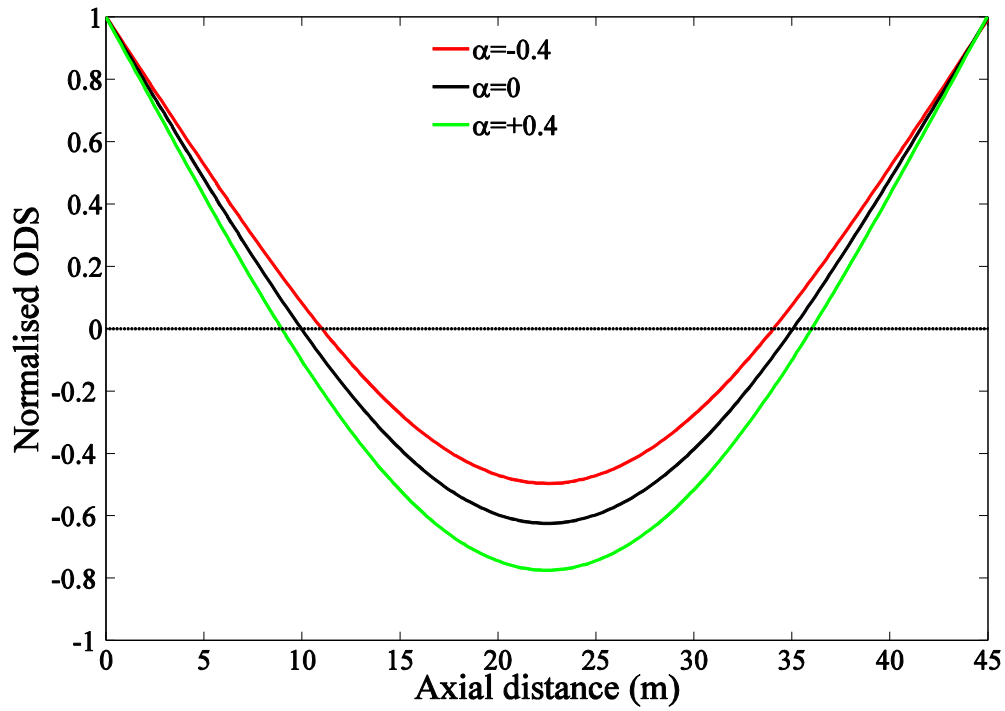


Figure 2. Operational deflection shapes at peak input power for the first bending mode, determined using the semi-analytical approach of the FE model with added water mass

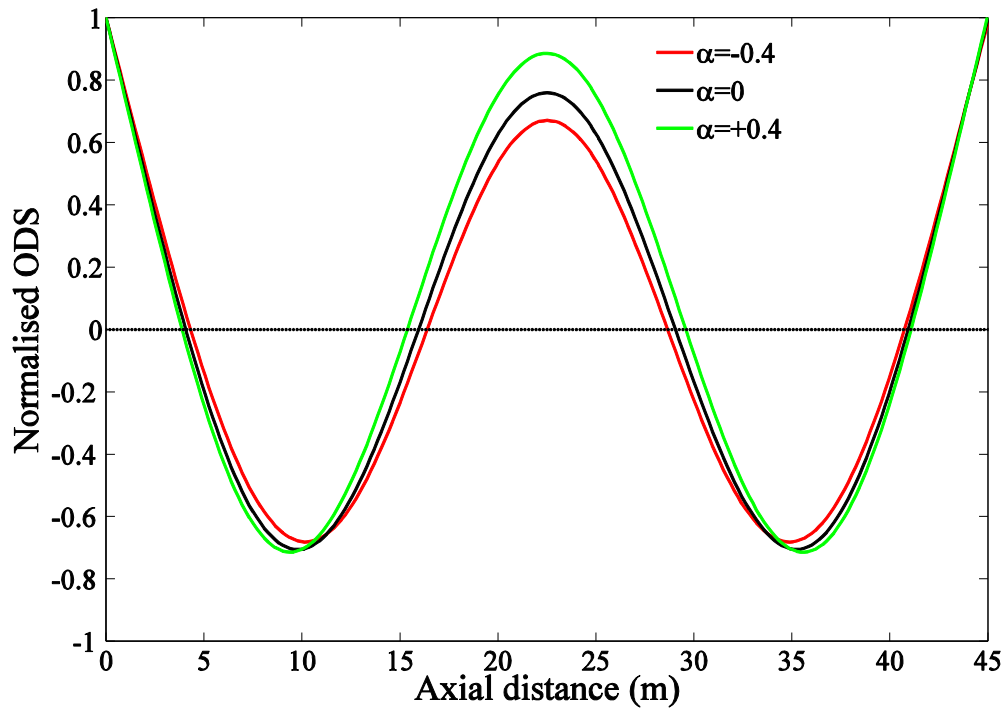


Figure 3. Operational deflection shapes at peak input power for the third bending mode, determined using the semi-analytical approach of the FE model with added water mass

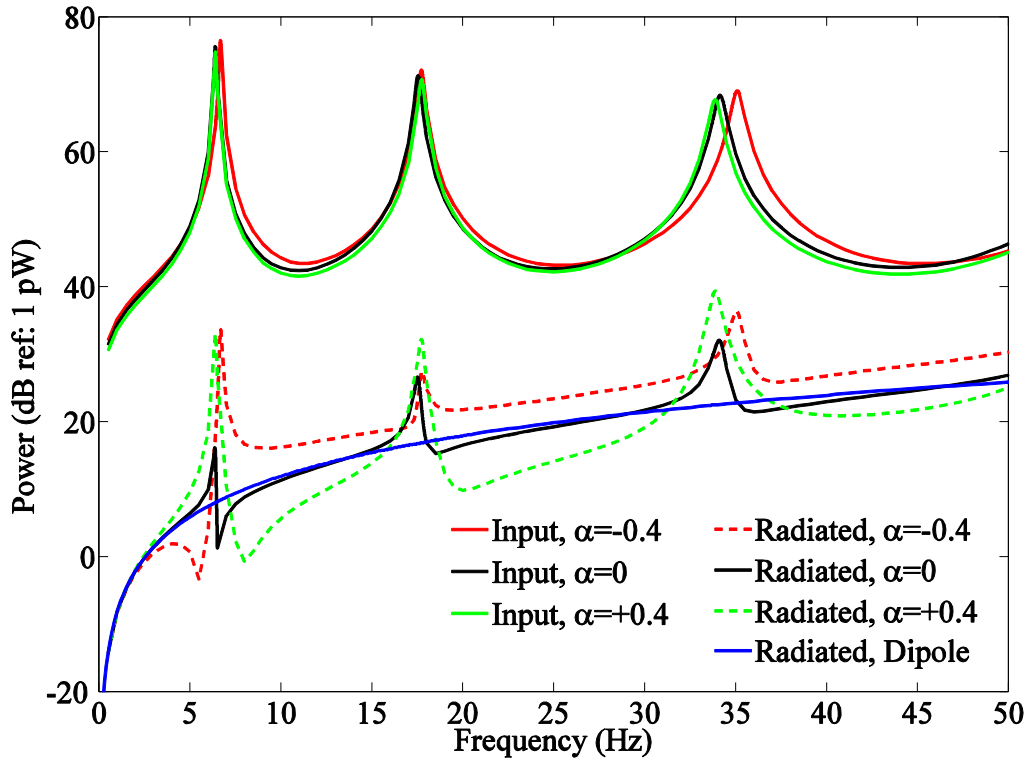


Figure 4. Input and radiated power, $\eta = 0.02$, determined using the fully coupled FE/BE model

6.4 Variation of peak input power and radiated sound power with variation in mass distribution

The variation of radiated sound power with α at the first and third resonant peaks is shown in Figs. 5 and 6, using the dipole as a reference for radiated sound power due to a unit applied force. Results are shown for both the semi-analytical approach and the fully coupled numerical approach, confirming that the simple FE model with assumed added water mass gives almost identical results to those from the coupled FE/BE model.

The peak frequencies for the first and third bending modes differ by a factor of more than five, so there is a marked difference in the importance of retarded time. The most striking result is at the first bending mode, where the radiated sound power varies by 20 dB in the range from $\alpha = -0.4$ to $\alpha = +0.4$, with a minimum for $\alpha \approx -0.05$. At this minimum, the radiation is same as that due to a simple dipole and the resonant vibration has almost no effect on sound power radiation. At the resonant frequency of about 6.3 Hz, the sound wavelength is over 5 times the length of the tube, so the effects of retarded time are small. The third bending mode is also symmetric, but the wavelength at 34 Hz is almost identical to the tube length and much larger retarded time effects are anticipated. The change in radiated sound power with mass distribution at the third bending mode is much weaker than for the first mode, but the directivity now varies strongly.

6.5 Directivity patterns at peak frequencies

Although overall radiated sound power is the simplest overall measure of the intensity of the radiated sound field, the directivity of the radiated sound field can contain peaks and nulls of considerable practical significance. Directivity patterns in the plane of the tube and applied force for the first and third bending modes are shown in Figs. 7 and 8 for $\alpha = -0.4, 0$ and $+0.4$. Following standard practice for representation of underwater noise signatures, these are presented as pressure levels at 1m from a point source that has the same far-field pressure distribution as the vibrating tube. Results from both FE and FE/BE models are shown. The directivity patterns are not exactly symmetrical about $\theta = 90^\circ$ because the ODSs are not pure mode shapes. In particular, they include both translational and rotational rigid

body motions. The agreement is very good in directions of highest pressure, but larger differences appear for directions where radiation is weak. This is likely to be due in part to the differences and numerical errors in calculated peak frequencies between the semi-analytical and numerical approaches, which change the effects of retarded time, and in part to end effects that are present in the numerical FE/BE model. The values of high pressures are practically of more importance than the values of low pressures. The out-of-plane pressure varies as $\sin \phi$, where ϕ is the angle of rotation about the tube axis for a given value of θ . Thus, the pressure amplitude is zero when $\phi = 0, 180^\circ$.

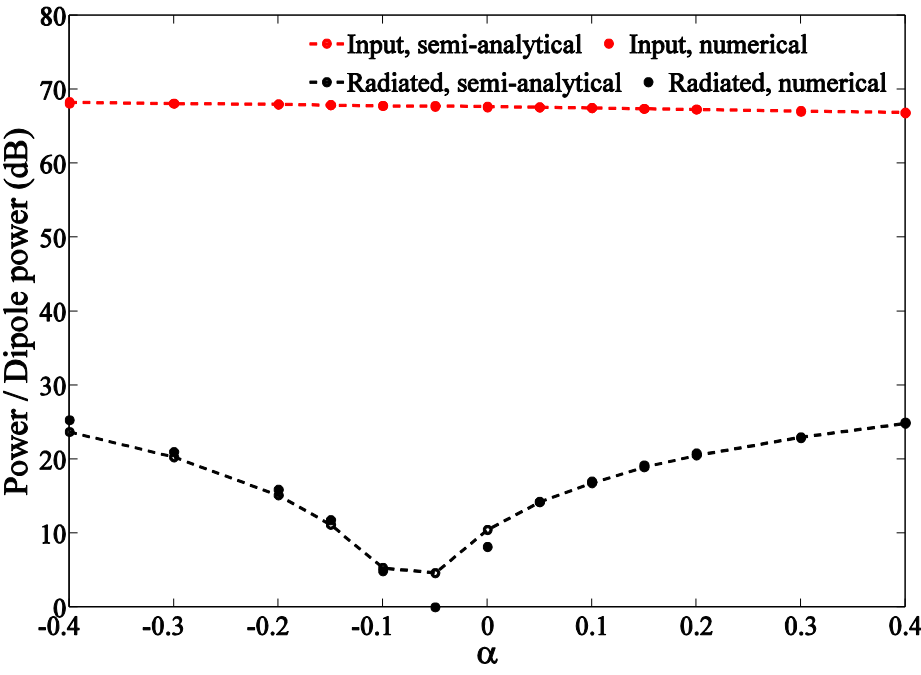


Figure 5. Input and radiated power at the first bending mode, determined using both the semi-analytical and numerical approaches

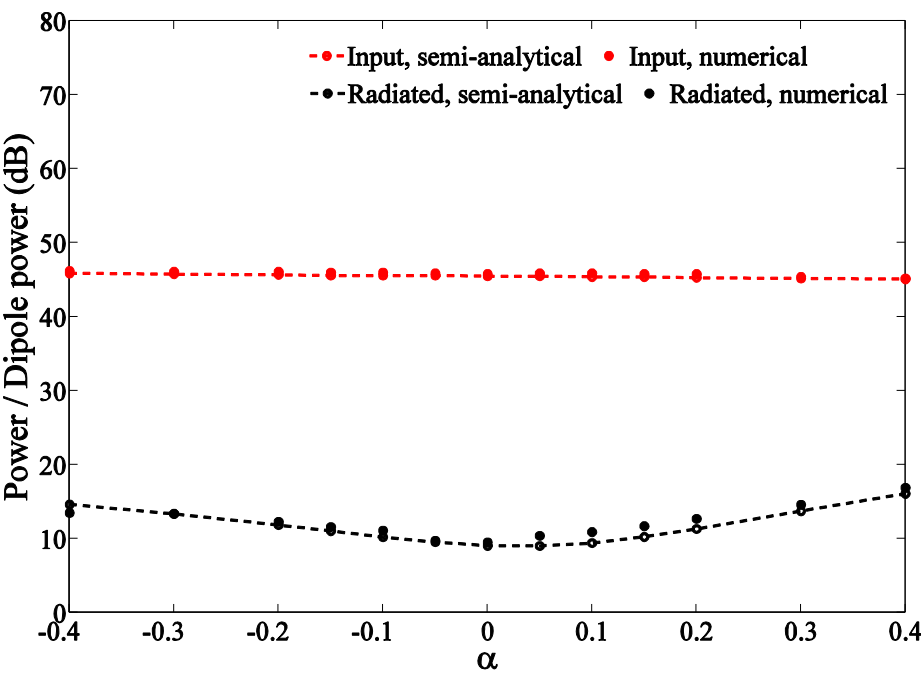


Figure 6. Input and radiated power at the third bending mode, determined using both the semi-analytical and numerical approaches

The directivity results for the first mode are close to those of an amplified dipole for $\alpha = -0.4$ to $\alpha = +0.4$ with weak lobes for $\alpha = 0$. This is the expected result when the wavelength of underwater sound is much greater than the length of the tube [3]. The directivity patterns show two major lobes for the second mode (not shown here) and three lobes for the third mode, that are particularly prominent for $\alpha = 0$. In some directions, the pressure level is lower than for a simple dipole. The strong dependence on α for the first and third modes is clearly apparent in Figs. 7 and 8.

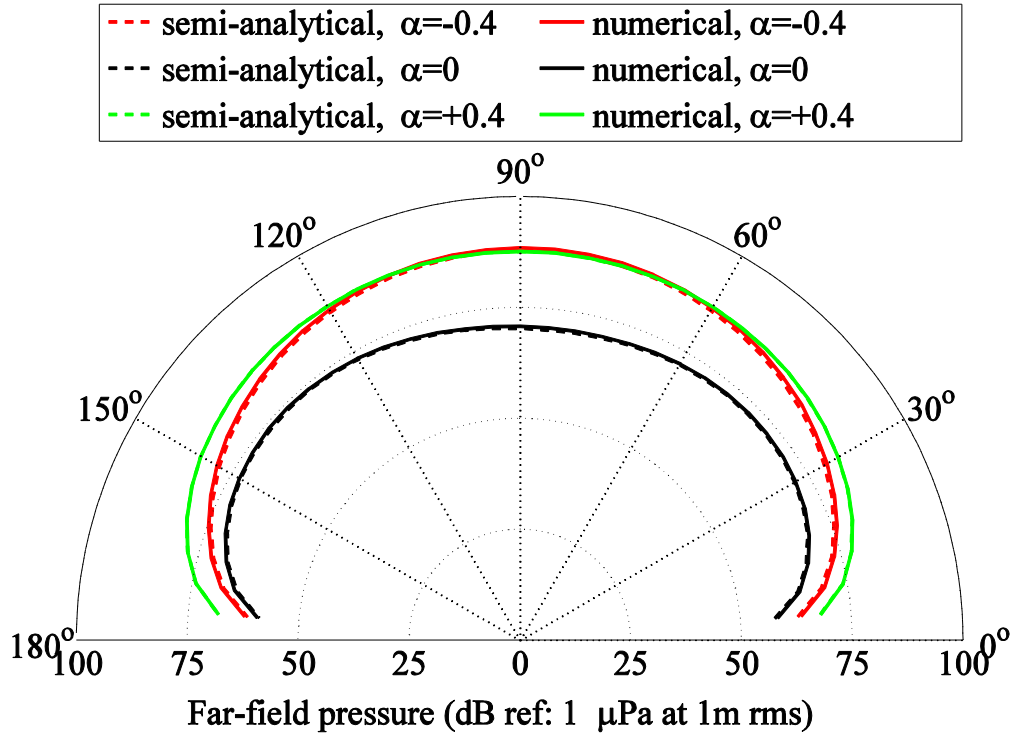


Figure 7. Directivity of the first bending resonance, determined using both the semi-analytical and numerical approaches

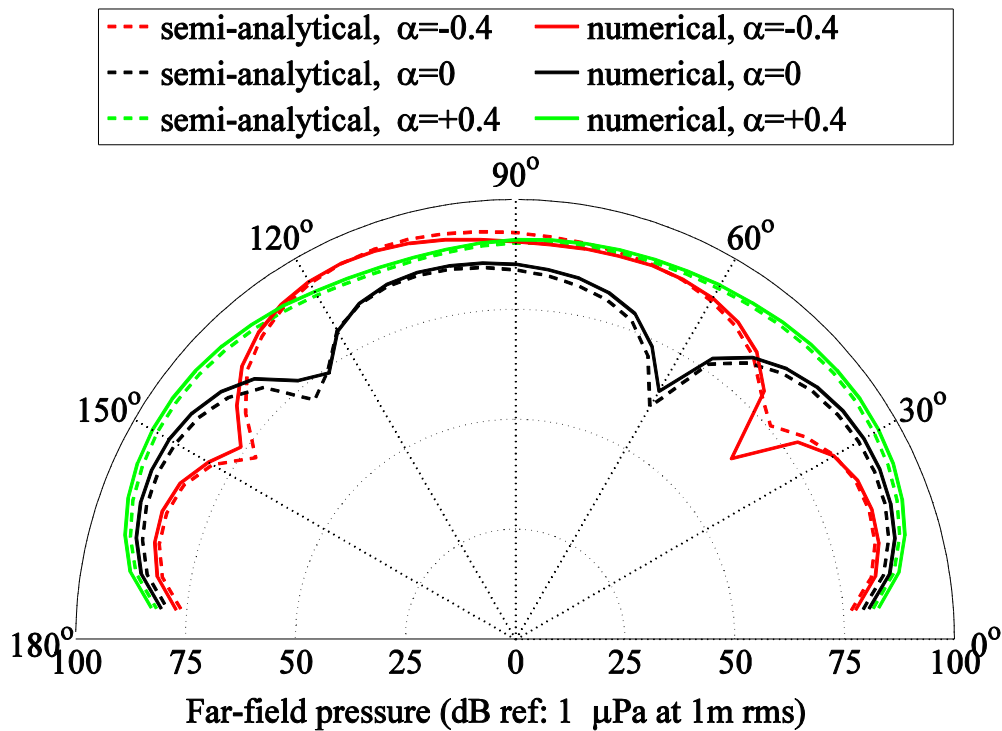


Figure 8. Directivity of the third bending resonance, determined using both the semi-analytical and numerical approaches

7. Summary

In this work, a semi-analytical approach involving a simple finite element model and a numerical approach involving a fully-coupled FE/BE model of a thin fluid-loaded tube in free-free vibration due to an applied fluctuating force at one end, for different longitudinal mass distributions, has been presented. Results from the semi-analytical and numerical approaches are compared in terms of resonant frequencies, operational deflection shapes, pressure fields in the plane of the tube and the total radiated sound power. The high aspect ratio of the tube ensured that any end effects are weak. The end effects were modelled in the FE/BE approach but ignored in the semi-analytical approach.

Results from the two approaches have shown almost identical predictions of the input power, radiated sound power and directivity of the far-field sound pressure. At very low frequencies, where the cylinder is rigid, underwater radiation has dipole characteristics. When the cylinder length is much less than a wavelength of underwater sound at a bending resonance, the directivity is similar to that of a simple dipole and the main effect of the resonance is to modify the dipole strength. When the wavelength is further reduced the effects of retarded time can have a powerful influence on directivity patterns due to bending mode resonances.

Variation in longitudinal mass distribution was shown to have only a weak influence on resonant frequencies and input power for the first three bending resonances of the tube, but to have a large effect on radiated sound power and directivity patterns.

Acknowledgement

The first author is grateful to Dr Malcolm Swinbanks for early insights into radiation from submerged cylinders when they were colleagues at YARD Ltd in Glasgow during the 1970s. Swinbanks recognised that the radiation due to bending resonances might be minimised by matching the axial distribution of mass and buoyancy in a submerged vessel.

References

- [1] Junger, M.C. “Radiation and scattering by submerged elastic structures”, *Journal of the Acoustical Society of America*, **57**(6), 1318-1326, (1975).
- [2] Junger, M.C. and Feit, D. *Sound, structures and their interaction*, MIT Press, 1985.
- [3] Junger, M.C. “Sound radiation by resonances of free-free beams”, *Journal of the Acoustical Society of America*, **52**(1), 332-334, (1972).
- [4] Peters, H., Kinns R. and Kessissoglou, N.J. “Effects of apparent mass on the radiated sound power from fluid-loaded structures”, *Ocean Engineering*, **105**, 83-91, (2015).
- [5] Peters, H., Kinns R. and Kessissoglou, N.J. “Effects of internal mass distribution and its isolation on the acoustic characteristics of a submerged hull”, *Journal of Sound and Vibration*, **333**(6), 1684-1697, (2014).
- [6] Hartnell-Beavis M.C. and Swinbanks, M.A. “Some recent practical and theoretical developments in noise reduction in ships”, *Proceedings of the Vibration and Noise Conference, Institute of Marine Engineers*, London, UK, 21 October 1976.
- [7] Kinns, R., Thompson, I.R.M, Kessissoglou, N.J. and Tso, Y. “Hull vibratory forces transmitted via the fluid and the shaft from a submarine propeller”, *Ships and Offshore Structures*, **2**(2), 183-189, (2007).
- [8] Korotkin, A.I. *Added masses of ship structures*, Springer Science, 2009.
- [9] Ross, D. *Mechanics of underwater noise*, Pergamon Press, 1976.